Original Article

Characteristics of altered biventricular hemodynamics after arterial switch operation for patients with d-transposition of the great arteries with preserved ejection fraction: a four-dimensional (4D) flow cardiovascular magnetic resonance (CMR) study

Li-Wei Hu[1,2#], Xin-Rong Liu[3#], Rong-Zhen Ouyang[1], Li-Jun Chen[4], Ai-Min Sun[1], Chen Guo[1], Xiao-Fen Yao[1], Yan-Yan Ma[1], Le Feng[1], Ting-Fan Wu[2], Qian Wang[1], Yu-Min Zhong[1,2]

[1]Department of Radiology, Shanghai Children's Medical Center, Shanghai Jiao Tong University School of Medicine, Shanghai, China; [2]PEDiatric Imaging Advanced Technology Research Center, Shanghai, China; [3]Department of Cardiothoracic Surgery, Shanghai Children's Medical Center, Shanghai Jiao Tong University School of Medicine, Shanghai, China; [4]Department of Pediatric Cardiology, Shanghai Children's Medical Center, Shanghai Jiao Tong University School of Medicine, Shanghai, China

Contributions: (I) Conception and design: LW Hu, YM Zhong; (II) Administrative support: Q Wang, YM Zhong; (III) Provision of study materials or patients: XR Liu, RZ Ouyang, LJ Chen; (IV) Collection and assembly of data: LW Hu, YY Ma, L Feng, C Guo, XF Yao, TF Wu; (V) Data analysis and interpretation: LW Hu, YM Zhong; (VI) Manuscript writing: All authors; (VII) Final approval of manuscript: All authors.

[#]These authors contributed equally to this work as co-first authors.

Correspondence to: Qian Wang, MD. Department of Radiology, Shanghai Children's Medical Center, Shanghai Jiao Tong University School of Medicine, 1678 Dongfang Road, Shanghai 200127, China. Email: wangqian@scmc.com.cn; Yu-Min Zhong, MD, PhD. Department of Radiology, Shanghai Children's Medical Center, Shanghai Jiao Tong University School of Medicine, 1678 Dongfang Road, Shanghai 200127, China; PEDiatric Imaging Advanced Technology Research Center, 1678 Dongfang Road, Shanghai 200127, China. Email: zyumin2002@163.com.

Background: The long-term monitoring of biventricular function is essential to identify potential functional decline in patients following the arterial switch operation (ASO). The underlying pathophysiological mechanisms responsible for altered biventricular hemodynamics in ASO patients are not yet well understood. This study sought to: (I) compare the biventricular kinetic energy (KE) and vorticity of ASO patients and age- and sex-matched controls; (II) investigate the associations of four-dimensional (4D) flow biventricular hemodynamics parameters and neo-aortic root dilation, supravalvular pulmonary stenosis, and pulmonary artery transvalvular pressure difference.

Methods: A total of 34 patients with dextro-transposition of the great arteries (D-TGA) who underwent ASO, and 17 age- and gender-matched healthy controls were prospectively recruited for this study. All the subjects underwent cine and 4D flow and late gadolinium enhancement scans, and all the patients underwent echocardiography within two weeks of cardiovascular magnetic resonance (CMR) imaging. The following four flow components were analyzed: direct flow, retained inflow, delayed ejection flow, and residual volume. In addition, the following six phasic blood flow KE parameters, normalized to the end-diastolic volume (EDV) and vorticity, were analyzed for both the left ventricle (LV) and right ventricle (RV): peak systolic phase, average systolic phase, peak diastolic phase, average diastolic phase, peak E-wave phase, and peak A-wave phase. The independent sample Student's *t*-test, Mann-Whitney U-test, univariable and multivariable stepwise regression analyses, intra and inter-observer variability analyses were used to compare patients and controls.

Results: In relation to the LV, the D-TGA patients had significantly decreased average vorticity, peak systolic vorticity, systolic vorticity, diastolic vorticity, and peak A-wave vorticity compared to the controls (all $P<0.01$). In relation to the RV, the pulmonary stenosis group had significantly increased peak E- and A-wave

kinetic energy normalized to the end-diastolic volume (KEi_{EDV}), and peak and average vorticity compared to the non-pulmonary stenosis group (all P<0.05). in the multivariable logistic regression model analysis, diastolic KEi_{EDV}, peak E-wave KEi_{EDV} peak A-wave $KEi_{EDV,}$ and average vorticity were associated a with transvalvular pressure difference (β=13.54, P<0.001 for diastolic KEi_{EDV}; β=105.26, P<0.001 for peak E-wave KEi_{EDV}; β=−49.36, P=0.027 for peak A-wave KEi_{EDV}; and β=−56.37, P<0.001 for average vorticity).

Conclusions: We found that 4D flow biventricular hemodynamics were more sensitive markers than the ejection fraction in the postoperative D-TGA patients. The RV diastolic KEi_{EDV} parameters and average vorticity were risk factors for pulmonary artery obstruction in the multivariable model.

Keywords: Transposition of great arteries; arterial switch operation (ASO); flow component; kinetic energy (KE); vorticity

Submitted Apr 25, 2024. Accepted for publication Aug 05, 2024. Published online Sep 21, 2024.
doi: 10.21037/qims-24-840
View this article at: https://dx.doi.org/10.21037/qims-24-840

Introduction

Dextro-transposition of the great arteries (D-TGA) is a cyanotic heart defect accounting for 5–7% of all congenital heart defects (CHDs) (1). Newborns with D-TGA can undergo corrective surgical repair early and survive to adulthood. In typical corrective surgery, called the arterial switch operation (ASO), the aorta and the pulmonary artery are translocated, and the coronary arteries are reimplanted into the neo-aorta (2). In the long term, the main complications of D-TGA treated by ASO are neo-aortic root dilatation and pulmonary artery obstruction (3-5). The continuous strict follow-up and monitoring of postoperative patients is essential to ensure the maintenance of ventricular function.

Echocardiography is the first-line imaging modality used for presurgical planning in children with D-TGA. Cardiovascular magnetic resonance (CMR) imaging provides comprehensive morphologic and ventricular functional information for CHD patients (6,7). Four-dimensional (4D) flow has been introduced as a novel tool for the visualization and quantification of flow in the heart and major blood vessels (8). 4D flow magnetic resonance imaging (MRI) with a time-dependent velocity vector field is able to depict hemodynamic characteristics, such as viscous energy loss (EL) and kinetic energy (KE), in individuals with tetralogy of Fallot (TOF) or Fontan palliation (9-12). It also has potential for use in comprehensive intraventricular fluid dynamic assessments of D-TGA patients.

D-TGA patients have excellent long-term overall survival after ASO. However, life-long monitoring of biventricular function by CMR imaging is required to detect potential functional deterioration long after ASO (13). Previous research has reported that the specific geometry of the ascending neo-aorta after ASO, including the Lecompte maneuver, is related to altered ascending aortic flow hemodynamics (14). However, the pathophysiological mechanisms for altered biventricular hemodynamics in ASO patients remain unknown. We hypothesized that biventricular hemodynamic parameters derived from 4D flow would be associated with postoperative adverse events in D-TGA patients with preserved ejection fraction (EF). In this study, we aimed to: (I) compare the biventricular KE and vorticity of ASO patients and age- and sex-matched controls; (II) investigate the associations of 4D flow biventricular hemodynamics parameters and neo-aortic root dilation, supravalvular pulmonary stenosis, and pulmonary artery transvalvular pressure difference. We present this article in accordance with the STROBE reporting checklist (available at https://qims.amegroups.com/article/view/10.21037/qims-24-840/rc).

Methods

Study subjects

In total, 104 D-TGA patients who underwent operation and 62 healthy controls were prospectively recruited for this study between July 2017 and August 2023. The patients underwent routine CMR examinations. The study flow chart is shown in *Figure 1*. To be eligible for inclusion in this study, the patients had to meet the following inclusion criteria: (I) be aged ≥3 or ≤18 years; (II) not have undergone any previous interventional management, such

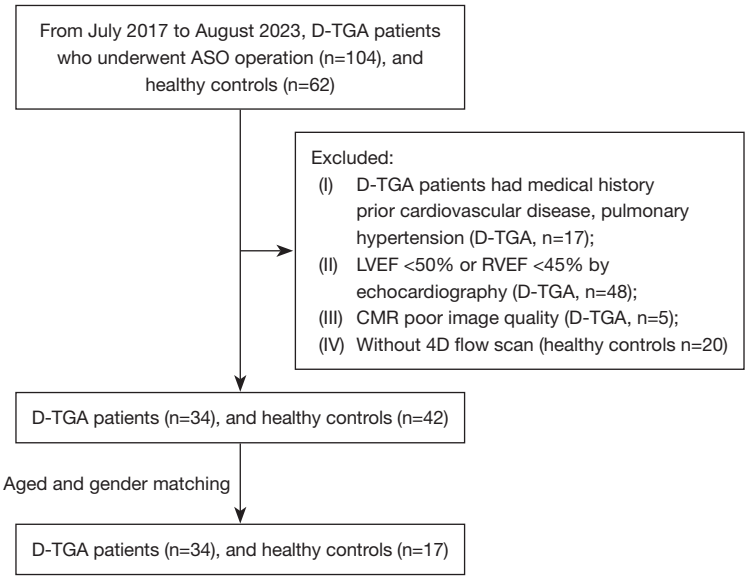

Figure 1 Flow chart showing recruitment of study subjects. D-TGA, dextro-transposition of the great arteries; ASO, arterial switch operation; LVEF, left ventricle ejection fraction; RVEF, right ventricle ejection fraction; CMR, cardiovascular magnetic resonance; 4D, four dimensional.

as re-intervention procedures, in the last three years; (III) have undergone assessment of neo-aortic root dilation, supravalvular pulmonary stenosis, and pulmonary artery transvalvular pressure difference by echocardiography in the two weeks before the CMR examination; and (IV) have preserved left ventricular ejection fraction (LVEF) >50% or right ventricular ejection fraction (RVEF) >45% by echocardiography. D-TGA patients were excluded from the study if they met any of the following exclusion criteria: (I) had a medical history of prior cardiovascular disease, pulmonary disease, or pulmonary hypertension; (II) had poor-quality CMR images or no 4D flow scans; and/or (III) had serious liver or kidney dysfunction. Additionally, 17 age- and sex-matched healthy control subjects were also recruited through our institutional website.

The study was conducted in accordance with the Declaration of Helsinki (as revised in 2013). All the patients or their legal guardians and the healthy control subjects provided written informed consent. The study was approved by the Institutional Medical Ethics Committee of Shanghai Children's Medical Center (No. SCMCIRB-K2022.49-1).

Echocardiography acquisition

The echocardiographic examination was performed using the Philips EPIQ 7C ultrasound machine (Philips, Andover, MA, USA) with a matrix array transducer (S5-1, S8-3). Previous research defined aortic dilatation as a Z-score >2.0 (15). The pulmonary supravalvar area and valve were imaged from the apical, parasternal, and subxiphoid windows. The diameter of the main pulmonary artery (MPA) was measured by echocardiography, and the stenosis of the MPA was graded based on its maximal velocity (Vmax) as follows: mild (2–3 m/s), moderate (3–4 m/s), or severe (>4 m/s) (16). Obstruction of the pulmonary artery was defined as the gradient of pressure of the MPA, and was calculated using the Bernoulli equation. Echocardiography was used to assess the transvalvular pressure difference according to the criteria described. This gradient was classified as mild (10–36 mmHg), moderate (36–64 mmHg), or severe (>64 mmHg) (*Figure 2*) (17).

CMR acquisition

All the subjects were scanned using a 3.0 Telsa system (Discovery MR750, GE, Chicago, IL, USA) using an 8- or 32-channel cardiac coil. The two-dimensional balanced steady state-free precession cine was used to evaluate biventricular function, and the parameters were as follows: repetition time (TR)/echo time (TE): 3.1/1.5 ms; acquisition matrix: (288–320)×(288–320); flip angle: 60°; slice thickness (no gap): 6–7 mm; and reconstructed cardiac phases: 30.

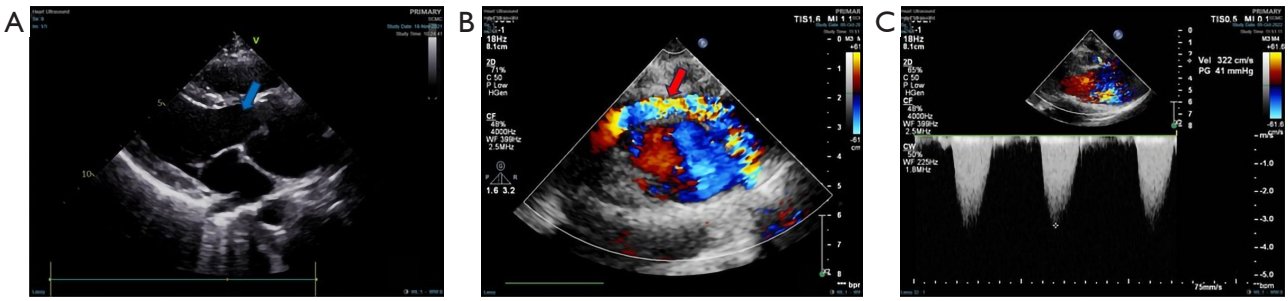

Figure 2 Evaluation of D-TGA vascular abnormalities using ultrasound color Doppler and blood flow. (A) Dilation of aortic sinus (blue arrow); (B) mild pulmonary artery stenosis (red arrow); (C) moderate obstruction of the pulmonary artery (41 mmHg). D-TGA, dextro-transposition of the great arteries.

Intravenous bolus injection of 0.2 mmol/kg gadopentetate dimeglumine for the contrast enhanced-magnetic resonance angiography (CE-MRA) was administered.

4D flow CMR datasets were acquired with retrospective electrocardiographic-gating during free-breathing. Three-dimensional cardiac cine with k-adaptive-t auto calibrating reconstruction for cartesian (kat ARC) was the prototype for the 4D flow imaging sequence based on the DV24 version. Full volumetric coverage of the two ventricles was provided from the transverse plane. The 4D flow CMR sequence parameters were as follows: TR/TE: 4.3/2.1 ms; volumetric element (voxel) size: (1.6–2.2)×(1.6–2.2)×(1.6–2.2) mm^3; flip angle: 15°; temporal resolution: 30 frames/cycle; acquired temporal resolution: 43–75 ms; reconstructed temporal resolution: 26–45 ms; velocity encoding: 120–160 cm/s (in accordance with the 4D flow consensus statement (18), the pulmonary artery obstruction cases used echocardiographic velocity to avoid aliasing artifacts); and parallel imaging reduction factor: R=8. The late gadolinium enhancement (LGE) parameters were as follows: TR/TE: 3.4/1.5 ms; field of view: 260–350 mm × 260–350 mm; flip angle: 35°; and slice thickness: 5–8 mm. LGE was assessed by late post-contrast imaging acquired 7–15 min (depending on heart rate) following contrast administration in the D-TGA group. The patients aged under eight years underwent the CMR examination with sedation, while the patients aged older than eight years, who were cooperative and could complete the CMR scan, as well as all the other subjects, underwent the CMR examination without sedation.

Cardiac function, valve regurgitation and LGE assessment

The epi- and endo-contours were drawn at the end-diastolic and end-systolic phase on the short-axis images for the left ventricle (LV) and right ventricle (RV). The mass, end-diastolic volume (EDV), stroke volume (SV), end-systolic volume (ESV), and EF were calculated using MASS (Leiden, The Netherlands). Mass, EDV, ESV, and SV were indexed by the body surface area (BSA). The indexed volumetric and mass variables were EDVi, ESVi, SVi, and massi. Aortic and pulmonary regurgitation were measured by 4D flow valve tracking in the D-TGA group with reference to those previously reported (8).

Intracardiac 4D flow CMR assessment

The contours of the endocardium and epicardium of the LV and RV underwent semi-automatic segmentation in all the short-axis heart phases. According to the contours, the pathline emission of the flow components, KE, and vorticity were analyzed using commercial software (MASS, Leiden, The Netherlands) (19). The hemodynamic parameters were obtained by averaging the KE value over the diastolic and systolic phases. The following definitions were adopted: (I) direct flow: blood that enters and exits the ventricle in the analyzed cardiac cycle; (II) retained inflow: blood that enters the ventricle but does not exit during the analyzed cycle; (III) delayed ejection flow: blood that starts and resides in the ventricle and exits during the analyzed cycle; and (IV) residual volume: blood that remains in the ventricle for at least two cardiac cycles.

For each voxel, the KE was calculated using the following formula:

$$KE = 1/2\ \rho\_blood \bullet V\_voxel \bullet v\_voxel^2 \quad [1]$$

where ρ_{blood} was the density of the blood (1.06 g/cm^3), V_{voxel} was the voxel volume, and v_{voxel} was the velocity magnitude of the corresponding voxel. For each phase, the total KE of

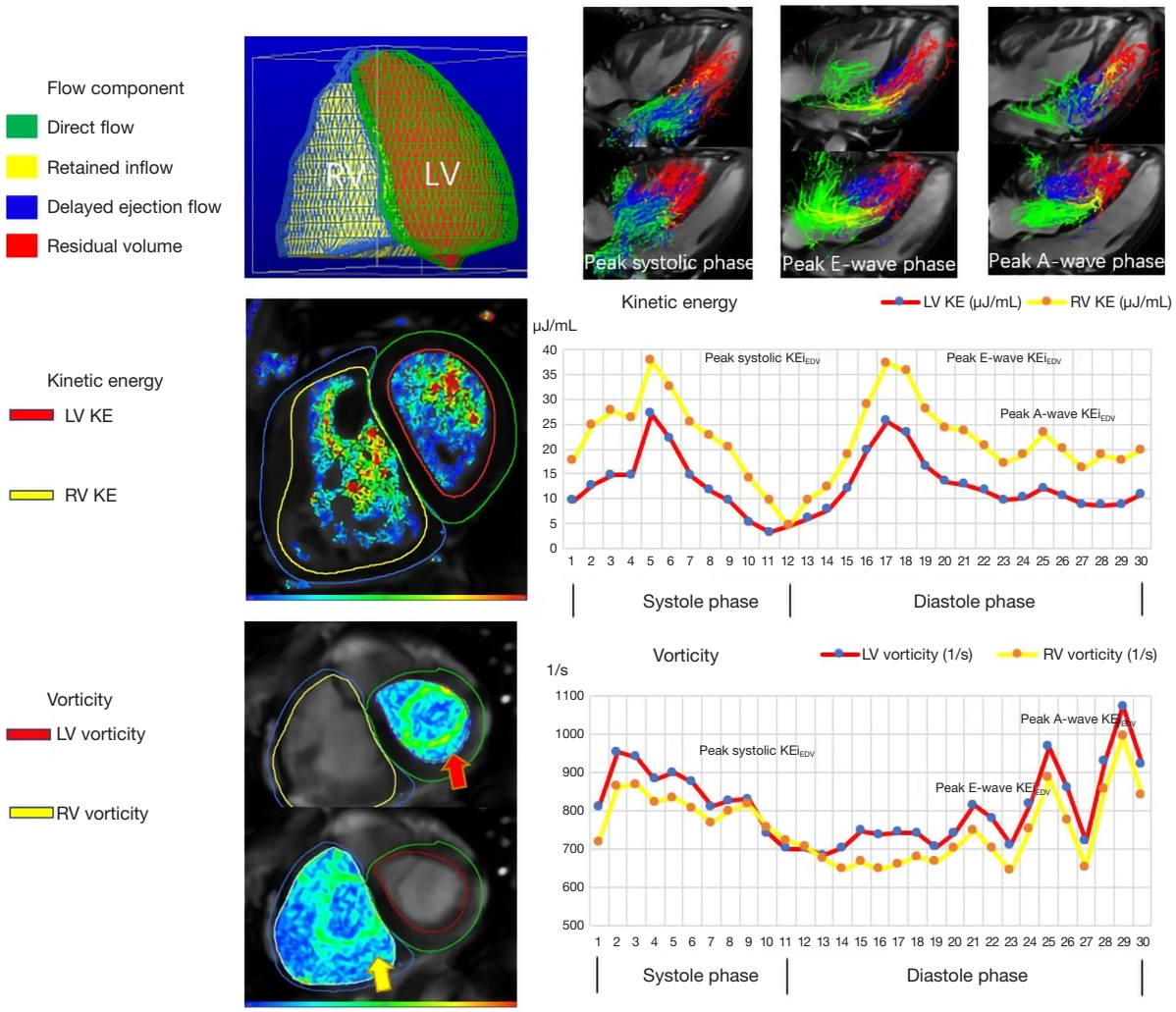

Figure 3 Four-chamber view with LV/RV particle tracing overlayed at the peak systole, peak early, and late diastolic filling phase in a 13-year-old male D-TGA patient. The corresponding LV/RV KEi_{EDV}. The LV/RV vorticity curve was described at one cardiac cycle. Red color: residual volume; blue color: delayed ejection flow; yellow color: retained inflow; green color: direct flow. The red arrow indicates the LV vortex ring on the short axis. The yellow arrow indicates the RV vortex ring on the short axis. LV, left ventricle; KE, kinetic energy; RV, right ventricle; D-TGA, dextro-transposition of the great arteries; KEi_{EDV}, kinetic energy normalized to end-diastolic volume; Peak systolic KEi_{EDV}, peak KEi_{EDV} of blood flow during systole; Systolic KEi_{EDV}, average KEi_{EDV} of blood flow during systole; Peak E-wave KEi_{EDV}, peak KEi_{EDV} of blood flow during early filling; Peak A-wave KEi_{EDV} peak KEi_{EDV} of blood flow during late filling.

the ventricle was obtained by adding the KE of every voxel. All the parameters were normalized to the KE ventricular end-diastolic volume (KEi_{EDV}) and reported accordingly in μJ/mL (20).

The components of the flow rotation were computed in each voxel of the segmented ventricular volumes. Since vorticity magnitude describes the local spinning motion of a fluid near a point, vorticity was expressed by the following formula:

$$\omega = \nabla \times V \quad [2]$$

where ∇ is the curl of its velocity field V, and was calculated using a compact derivative algorithm (21).

Time-resolved KE and vorticity curves were generated to derive physiologically relevant parameters (*Figure 3*).

Statistical analysis

The data were presented as the median (interquartile

range) or number (%). The *t*-test was used to compare the normally distributed variables, and the Mann-Whitney U-test was used to compare the non-normally distributed variables between the D-TGA patients and controls. Based on the previously described adverse outcomes of the D-TGA patients, a univariate analysis was conducted using a prior selection of explanatory variables. The stepwise regression algorithm was introduced, and Akaike information criterion was used as the screening quantitative index. Based on multicollinearity, the parameters were incorporated into the multivariable model. The association between the variables was expressed as the 95% confidence interval (CI). The intraclass correlation coefficient (ICC) and coefficient of variation (COV) were used to assess the intra- and inter-observer agreements in all the 4D flow parameters using five random patients and five random subjects. A P value <0.05 was considered statistically significant.

Results

Participant characteristics and myocardial function

The demographic, morphological, and functional characteristics of the subjects are set out in *Table 1*. There was no significant difference between the D-TGA patients and controls in this study in terms of age. The median CMR postoperative follow-up time was 8.3 years. The study included D-TGA patients with intact ventricular septum (14 cases), and D-TGA patients with ventricular septal defects (VSDs) (20 cases). Five patients underwent valvuloplasty or balloon pulmonary angioplasty after ASO. Of the patients, 25 had neo-aortic root dilation, and 25 had obstruction of the pulmonary artery, including 16 cases of supravalvular pulmonary stenosis. The D-TGA patients were significantly smaller than the controls in terms of height, weight, and BSA, and had a significantly lower heart rate (all P<0.05, *Table 1*). There were no statistically significant differences between the two groups in terms of EDVi, ESVi, SVi, and EF in the LV and RV (*Table 1*). LV massi, RV massi, and the RVEDV/LVEDV ratio did not differ significantly between the two groups. Among the patients, 24 had aortic valve regurgitation (6%), 32 had pulmonary valve regurgitation (10%), and 2 (6%) had positive myocardial LGE.

Changes in the flow components, KE, and vorticity profiles

All the included subjects had good quality 4D flow CMR data, as confirmed by a valid count of 80–99%.

In relation to the LV, the D-TGA patients had significantly lower values than the controls in terms of the retained inflow, average KEi_{EDV}, peak systolic KEi_{EDV}, systolic KEi_{EDV}, peak E-wave KEi_{EDV}, and peak A-wave KEi_{EDV} (all P<0.05, *Table 2* and *Figures 4*,*5*). The D-TGA patients had significantly decreased average vorticity, peak systolic vorticity, systolic vorticity, peak A-wave vorticity, and diastolic vorticity than the controls (all P<0.01, *Table 3* and *Figure 6*).

In relation to the RV, the D-TGA patients differed significantly in all the flow component parameters and KE parameters compared to the controls (all P<0.001, *Table 2*), except diastolic KEi_{EDV} (P=0.452; *Figures 4*,*5*). In terms of the vorticity parameters, the D-TGA patients did not differ significantly from the controls (all P>0.05, *Table 3* and *Figure 6*). A significant increase was observed in the peak E-wave KEi_{EDV} of the D-TGA patients with supravalvular pulmonary stenosis (P=0.042, *Table 4*). There was also a significant increase in the average vorticity, peak systolic vorticity, and systolic vorticity between the supravalvular and non-supravalvular pulmonary stenosis patient subgroups (all P<0.05, *Table 4*).

Association between the RV 4D flow parameters and pulmonary artery obstruction

In the univariate analysis, all the KEi_{EDV} parameters were associated with a transvalvular pressure difference (r=12.64, P<0.001 for the average KEi_{EDV}; r=8.45, P=0.021 for the systolic KEi_{EDV}; r=10.54, P=0.003 for the systolic KEi_{EDV}; r=10.81, P=0.002 for the peak E-wave KEi_{EDV}; r=10.29, P=0.004 for the peak E-wave KEi_{EDV}; and r=9.32, P=0.010 for the peak A-wave KEi_{EDV}; *Table 5*).

In the multivariate analysis, the diastolic KEi_{EDV}, peak E-wave KEi_{EDV} peak A-wave $KEi_{EDV,}$ and average vorticity were associated with a transvalvular pressure difference (β=13.54, P<0.001 for the diastolic KEi_{EDV}; β=105.26, P<0.001 for the peak E-wave KEi_{EDV}; β=–49.36, P=0.027 for the peak A-wave KEi_{EDV}; β=–56.37, P<0.001 for average vorticity; *Table 5*).

Reproducibility

Additionally, 10 randomly selected subjects were used to assess the reproducibility of the blood flow components, KE, and vorticity parameters. The respective ICC for intra-observer variability was 89.1–99.8% and that for inter-observer variability was 84.9–96.8%. The respective COV for intra-observer variability was 2.6–11.5 and that for inter-observer variability was 4.4–13.5 (*Table 6*).

Table 1 Comparison of the demographic characteristics, and LV and RV function between the D-TGA patients and controls

Parameters	D-TGA (n=34)	Control (n=17)	P
Demographic			
Age at CMR scan (years)	9.5 [6.4, 13.7]	10.0 [8.5, 11.9]	0.622
Time after primary repair (years)	8.3 [4.8, 12.2]	–	–
Gender, M/F (n)	20/14	10/7	>0.99
Height (cm)	125 [111.5, 152]	148 [137, 153]	0.013
Weight (kg)	23.35 [18.72, 37.5]	39 [29.2, 46.5]	0.015
Body surface area (m^2)	0.9 [0.6, 1.1]	1.27 [1.1, 1.4]	0.001
Heart rate (bpm)	70.5 [60.8, 81.5]	77.0 [73.0, 93.5]	0.022
Transposition type			
D-TGA-IVS	14 [41]	–	–
D-TGA-VSD	20 [59]	–	–
Cases with re-intervention	5 [15]	–	–
Echocardiographic parameters			
Aortic dilatation	25 [73]		
Supravalvular pulmonary stenosis (m/s)	2.3 [1.8, 2.7]		
Mild	12 [35.2]		
Moderate	3 [8.8]		
Severe	1 [2.9]		
Obstruction of the pulmonary artery (mmHg)	17.0 [9.8, 31.5]		
Mild	18 [53]		
Moderate	5 [14.7]		
Severe	2 [5.8]		
LV function			
LV EDV index (mL/m^2)	79.8 [75.2, 90.0]	75.7 [64.8, 89.3]	0.304
LV ESV index (mL/m^2)	32.0 [29.6, 36.0]	29.0 [27.8, 36.0]	0.405
LV SV index (mL/m^2)	49.4 [43.9, 55.0]	46.6 [40.4, 54.8]	0.426
LV ejection fraction (%)	60.5 [55.4, 63.7]	61.1 [56.5, 64.0]	0.976
LV mass index (g/m^2)	42.8 [38.7, 50.0]	42.7 [34.7, 47.8]	0.300
RV function			
RV EDV index (mL/m^2)	85.3 [76.4, 96.5]	82.8 [78.2, 94.6]	0.865
RV ESV index (mL/m^2)	33.4 [28.9, 38.2]	36 [32.2, 43.1]	0.255
RV SV index (mL/m^2)	49.7 [43.3, 60]	48.4 [45.3, 52.4]	0.410
RV ejection fraction (%)	59.0 [55.3, 61.6]	56.1 [53.6, 59.6]	0.135
RV mass index (g/m^2)	26.37 [22.99, 35.06]	27.45 [24.32, 31.23]	0.988
RVEDV/LVEDV ratio	1.03 [0.96, 1.13]	1.10 [1.03, 1.17]	0.485

Table 1 *(continued)*

Table 1 *(continued)*

Parameters	D-TGA (n=34)	Control (n=17)	P
Valve regurgitation and late gadolinium enhancement			
Aortic valve regurgitation	24 [70.6]	–	–
Pulmonary valve regurgitation	32 [94.1]	–	–
Myocardial delayed enhancement	2 [6]		

The data are presented as the median [IQR] or n [%]. IQR = [25th percentile, 75th percentile]. LV, left ventricle; RV, right ventricle; D-TGA, dextro-transposition of the great arteries; CMR, cardiovascular magnetic resonance; M/F, male/female; IVS, intact ventricular septum; VSD, ventricular septal defect; EDV, end-diastolic volume; ESV, end-systolic volume; SV, stroke volume; RVEDV, right ventricle end-diastolic volume; LVEDV, left ventricle end-diastolic volume; IQR, interquartile range.

Table 2 Comparison of the flow components and KE of the 4D flow parameters between the D-TGA patients and controls.

Parameters	D-TGA (n=34)	Control (n=17)	P
LV 4D flow			
Direct flow (%)	32.5 [28.0, 35.9]	33.2 [30.0, 37.1]	0.447
Retained inflow (%)	12.3 [10.4, 18.6]	19.8 [14.3, 25.4]	0.007
Delayed ejection flow (%)	23.5 [18.6, 25.6]	20.4 [15.0, 22.3]	0.060
Residual volume (%)	26.7 [22.4, 31.8]	23.4 [18.0, 30.5]	0.140
Average KEi_{EDV} (μJ/mL)	8.6 [7.3, 11.7]	11.0 [9.9, 13.9]	0.004
Peak systolic KEi_{EDV} (μJ/mL)	17.6 [11.2, 23.3]	24.2 [21.8, 29.5]	0.020
Systolic KEi_{EDV} (μJ/mL)	7.6 [5.8, 10.4]	11.3 [9.5, 14.8]	<0.001
Diastolic KEi_{EDV} (μJ/mL)	10.3 [8.5, 13.0]	12.3 [9.5, 14.3]	0.124
Peak E-wave KEi_{EDV} (μJ/mL)	11.5 [9.9, 13.6]	27.0 [17.2, 29.7]	<0.001
Peak A-wave KEi_{EDV} (μJ/mL)	7.9 [4.4, 10.6]	11.6 [9.2, 13.2]	0.003
RV 4D flow			
Direct flow (%)	35.2 [30.3, 37.7]	41.8 [34.9, 45.4]	<0.001
Retained inflow (%)	20.2 [14.9, 24.0]	15.0 [12.6, 18.3]	<0.001
Delayed ejection flow (%)	15.5 [12.7, 19.6]	18.2 [19.0, 26.9]	<0.001
Residual volume (%)	28.7 [26.0, 34.3]	23.1 [20.2, 26.3]	<0.001
Average KEi_{EDV} (μJ/mL)	6.8 [5.9, 8.1]	10.9 [9.9, 14.5]	<0.001
Peak systolic KEi_{EDV} (μJ/mL)	14.4 [10.0, 17.9]	28.7 [25.9, 33.3]	<0.001
Systolic KEi_{EDV} (μJ/mL)	6.9 [5.0, 8.6]	16.4 [12.0, 17.7]	<0.001
Diastolic KEi_{EDV} (μJ/mL)	7.4 [6.2, 9.2]	7.2 [6.4, 10.5]	0.452
Peak E-wave KEi_{EDV} (μJ/mL)	7.6 [6.3, 9.1]	11.0 [9.3, 15.6]	<0.001
Peak A-wave KEi_{EDV} (μJ/mL)	6.8 [4.9, 8.7]	9.5 [7.5, 11.9]	0.002
KE discordance	0.9 [0.9, 1.1]	1.3 [1.1, 1.6]	<0.001

The data are presented as the median [IQR]. IQR = [25th percentile, 75th percentile]. KE, kinetic energy; 4D, four dimensional; D-TGA, dextro-transposition of the great arteries; LV, left ventricle; KEi_{EDV}, kinetic energy normalized to EDV; Peak systolic KEi_{EDV}, peak KEi_{EDV} of blood flow during systole; Systolic KEi_{EDV}, average KEi_{EDV} of blood flow during systole; Peak E-wave KEi_{EDV}, peak KEi_{EDV} of blood flow during early filling; Peak A-wave KEi_{EDV}, peak KEi_{EDV} of blood flow during late filling; RV, right ventricle; KE discordance, RV/LV systolic KEi_{EDV}; EDV, end-diastolic volume; IQR, interquartile range.

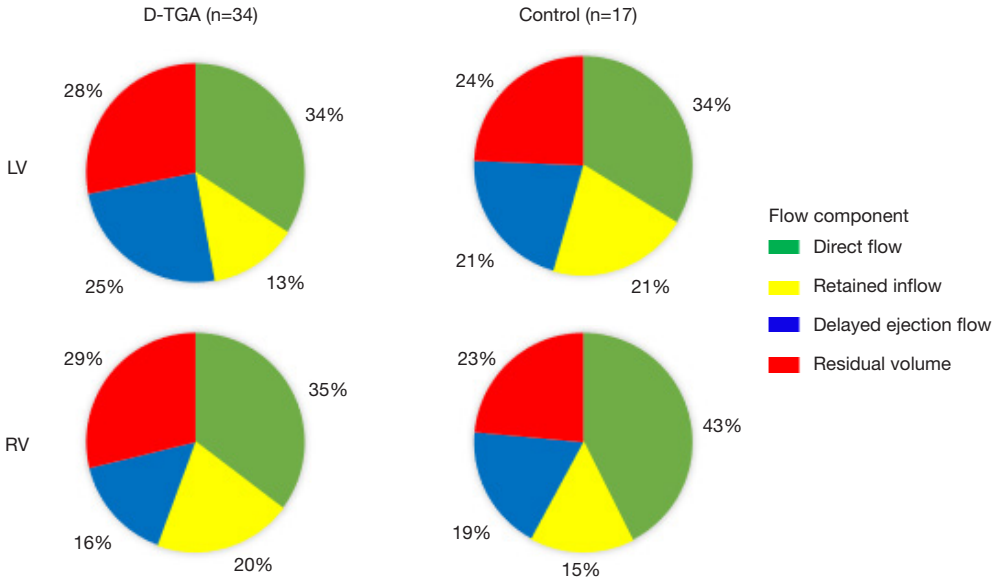

Figure 4 Comparison of the blood flow components of both ventricles between the D-TGA group and control group. LV, left ventricle; RV, right ventricle; D-TGA, dextro-transposition of the great arteries.

Discussion

Main findings

Currently, 4D flow CMR imaging allows for the visualization and quantification of abnormal hemodynamics, which has led to better knowledge of cardiovascular hemodynamics and disease progression in CHD patients (22,23). Previous studies have assessed hemodynamic vorticity in Fontan patients and volunteers (24-26). This was the first 4D flow CMR study to investigate biventricular vorticity for D-TGA patients. The main findings of the study are as follows: (I) some LV and RV flow components and the KEi_{EDV} parameters differed significantly between two groups; (II) LV systolic vorticity, diastolic vorticity, and peak A-wave vorticity differed significantly between the two groups. (III) The supravalvular pulmonary stenosis subgroup had significantly higher RV systolic vorticity and peak E-wave KEi_{EDV} than non-supravalvular pulmonary stenosis group; and (IV) all the RV diastolic KEi_{EDV} parameters and RV average vorticity were risk factors for pulmonary artery obstruction.

LV and RV hemodynamics are more sensitive markers than EF

In our study, the LV and RV of the D-TGA patients exhibited normal cardiac function and did not differ significantly compared to the control group during aortic and pulmonary mild valve regurgitation. Previous studies (17) have shown that patients with D-TGA generally maintain biventricular function similar to that of controls in a medium-term follow-up period of less than 20 years after ASO. Our study included younger subjects than previous studies; the median age of the patients in the D-TGA group was 9.5 years, and that of the control group was 10.0 years. These findings align with the results of previous research (17).

In total, 64% of the patients had aortic valve regurgitation in our study. The presence of aortic valve regurgitation and neo-aortic root dilation altered the proportion of the flow component. Significant differences were observed in the retained inflow of the LV between the two groups, with percentages of 12.3% and 19.8%, respectively. Previous research has shown that the retained inflow needs to decelerate at the end of diastole, so that additional KE can subsequently be acquired before ejection during a subsequent systole in a normal LV (27). It may be that the decreased proportion of the LV retained inflow decreases its ability of accelerate blood compared to a normal LV. Grotenhuis *et al.* (28) examined biventricular systolic and diastolic dysfunction in patients with D-TGA patients, and found that parts of the biventricular flow components, especially the RV, differed significantly between the two groups Thus, the hemodynamics

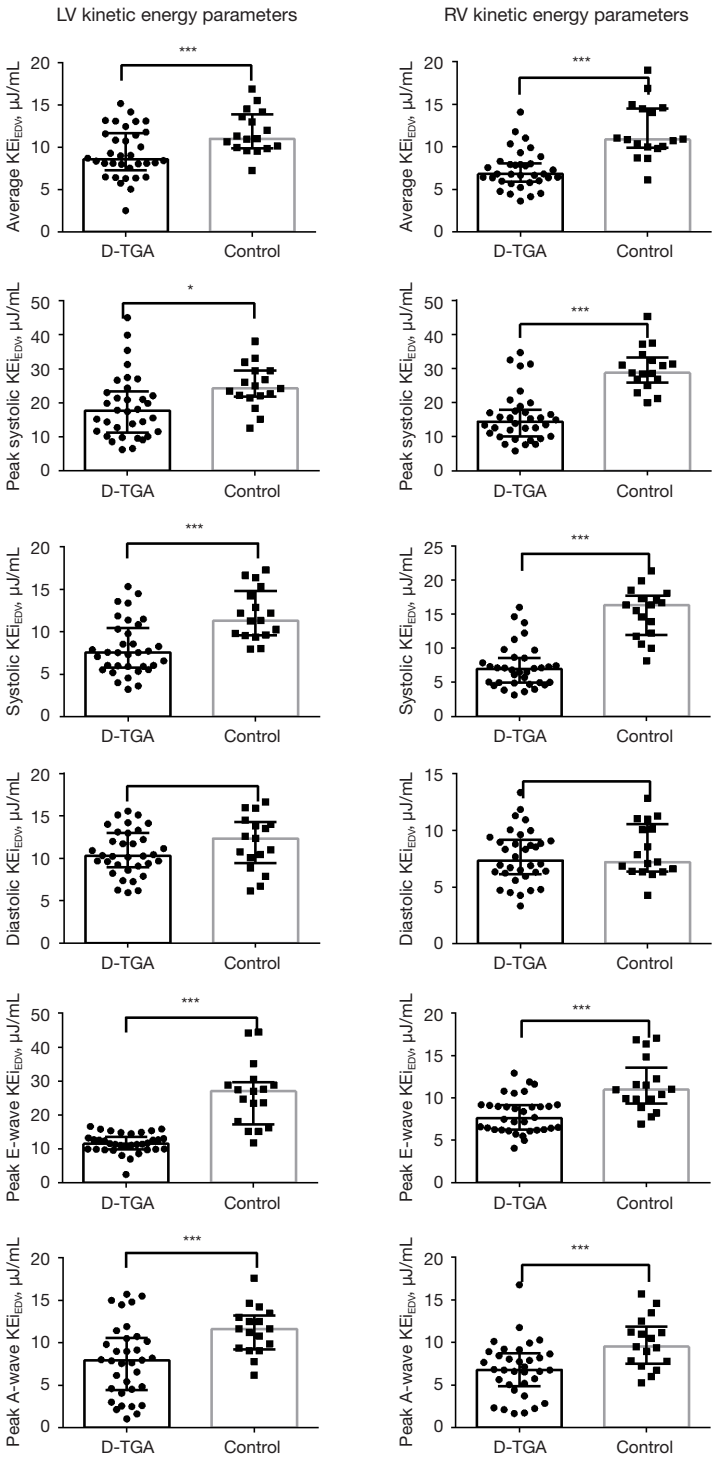

Figure 5 Comparison of the kinetic energy of both ventricles between the D-TGA group and the control group. *, P<0.05 compared with healthy controls; ***, P<0.001 compared with healthy controls. LV, left ventricle; RV, right ventricle; D-TGA, dextro-transposition of the great arteries; KEi_{EDV}, kinetic energy normalized to end-diastolic volume.

Table 3 Comparison of the vorticity parameters between the D-TGA patients and controls

Parameters	D-TGA (n=34)	Control (n=17)	P
LV 4D flow			
Average vorticity (1/s)	502.0 [376.1, 623.3]	639.5 [549.5, 732.0]	0.004
Peak systolic vorticity (1/s)	628.9 [514.2, 722.8]	866.4 [736.3, 963.3]	<0.001
Systolic vorticity (1/s)	478.2 [338.6, 639.3]	673.9 [582.3, 735.7]	0.001
Diastolic vorticity (1/s)	527.7 [396.6, 631.1]	624.7 [528.7, 729.2]	0.01
Peak E-wave vorticity (1/s)	528.6 [407.5, 630.6]	605.0 [508.4, 700.6]	0.076
Peak A-wave vorticity (1/s)	528.2 [353.9, 654.3]	693.5 [567.4, 780.1]	<0.001
RV 4D flow			
Average vorticity (1/s)	461.0 [334.7, 584.4]	512.6 [454.4, 559.9]	0.542
Peak systolic vorticity (1/s)	575.4 [426.5, 677.3]	629.8 [564.3, 707.8]	0.407
Systolic vorticity (1/s)	457.3 [330.3, 610.1]	541.7 [482.1, 585.1]	0.271
Diastolic vorticity (1/s)	468.1 [351.5, 579.0]	470.8 [415.7, 514.3]	0.798
Peak E-wave vorticity (1/s)	469.7 [358.1, 569.5]	444.1 [404.8, 480.6]	0.345
Peak A-wave vorticity (1/s)	446.9 [324.8, 599.4]	493.3 [440.2, 542.2]	0.593

The data are presented as the median [IQR]. IQR = [25th percentile, 75th percentile]. D-TGA, dextro-transposition of the great arteries; LV, left ventricle; 4D, four dimensional; RV, right ventricle; IQR, interquartile range.

parameters are more sensitive markers than EF in evaluating systolic and diastolic dysfunction (see also the previous review (29).

The value of LV hemodynamics in myocardial remodeling

The LV average KEi_{EDV}, peak systolic KEi_{EDV}, systolic KEi_{EDV}, peak E-wave KEi_{EDV}, and peak A-wave KEi_{EDV} of the D-TGA patients were found to be significantly lower than those of the controls. This could be attributed to two main factors. First, the altered aortic geometry may result in increased LV afterload, leading to decreased LV hemodynamic efficiency (26). Second, it is possible that the myocardial tissue in D-TGA patients has experienced early damage due to perinatal cyanosis and cardioplegia. It should be noted that the potential influence of other factors could not be excluded in our study.

Grotenhuis *et al.* examined diffuse myocardial fibrosis of the LV in D-TGA patients using T1 relaxometry CMR imaging, and reported that it was correlated with the LV mass/volume ratio (R=0.60, P<0.001) (28). In D-TGA patients, subclinical signs of ventricular and myocardial remodeling are present, including increased LV dimensions and signs of LV fibrosis. There were no significant differences in the LV mass index and RVEDV/LVEDV ratio in D-TGA patients and controls. It may be that LV remodeling needs to be assessed over a longer period in the future.

The characteristics of KE and vorticity in D-TGA

KE is a crucial component of the heart's external work, and is responsible for accelerating blood from a resting state to its current velocity (30). Callaghan *et al.* (31) conducted a study using 4D-flow MRI to examine the biventricular hemodynamics in patients with arterial and atrial switch D-TGA and normal subjects, and observed that increased EL leads to alterations in decreased KE. In our study, we observed significant differences in the RV KEi_{EDV} parameters with normal cardiac function, except diastolic KEi_{EDV}. Compared to the LV, the RV is more susceptible to disruption and disorder, primarily because morphologically, it is characterized by a fused inflow and a highly spherical ventricle.

Vorticity is commonly defined as the curl of a fluid velocity vector. Our previous research showed that the presence of vortices in the ventricular blood volume may serve as an indicator of enhanced cardiac efficiency (32).

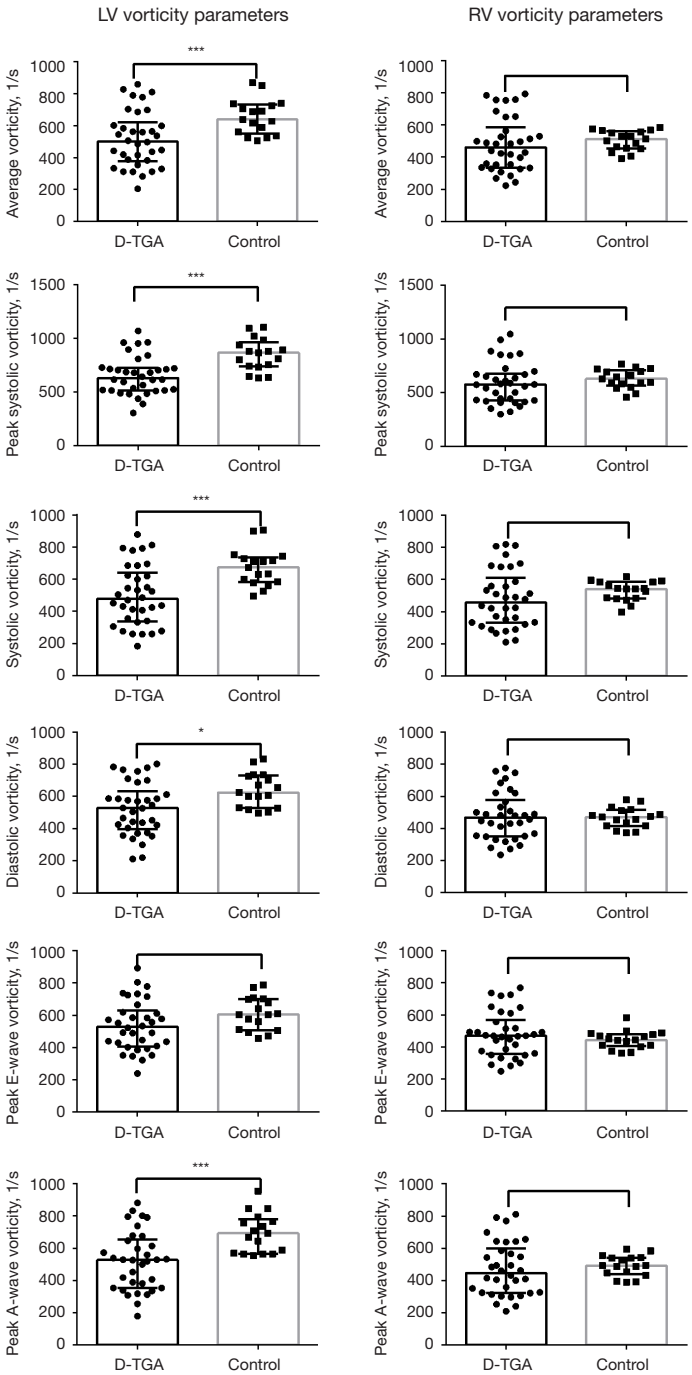

Figure 6 Comparison of the vorticity of both ventricles between the D-TGA group and the control group. *, P<0.05 compared with healthy controls; ***, P<0.001 compared with healthy controls. LV, left ventricle; RV, right ventricle; D-TGA, dextro-transposition of the great arteries.

Table 4 Comparison of the 4D flow parameters between supravalvular pulmonary stenosis and non-supravalvular pulmonary stenosis in D-TGA

Parameters	Supravalvular pulmonary stenosis (n=16)	Non-supravalvular pulmonary stenosis (n=18)	P
Direct flow (%)	35.5 [26.1, 37.4]	34.8 [30.8, 38.2]	0.739
Retained inflow (%)	20.2 [14.8, 24.7]	20.7 [15.3, 24.0]	0.780
Delayed ejection flow (%)	15.0 [10.3, 23.0]	15.7 [12.9, 17.1]	0.901
Residual volume (%)	29.0 [23.0, 35.5]	28.6 [26.6, 33.6]	0.939
Average KEi_{EDV} (μJ/mL)	7.42 [6.1, 9.8]	6.65 [5.6, 7.9]	0.125
Peak systolic KEi_{EDV} (μJ/mL)	17.1 [12.5, 20.6]	13.1 [9.4, 15.6]	0.093
Systolic KEi_{EDV} (μJ/mL)	7.5 [5.2, 10.9]	6.7 [4.9, 7.3]	0.116
Diastolic KEi_{EDV} (μJ/mL)	8.7 [6.3, 10.0]	7.0 [5.9, 8.7]	0.175
Peak E-wave KEi_{EDV} (μJ/mL)	9.0 [6.5, 10.7]	6.8 [6.2, 8.9]	0.042
Peak A-wave KEi_{EDV} (μJ/mL)	8.1 [4.2, 9.1]	6.6 [4.9, 7.7]	0.235
Average vorticity (1/s)	489.3 [401.8, 705.1]	391.3 [326.7, 557.2]	0.018
Peak systolic vorticity (1/s)	593.1 [498.9, 803.1]	509.2 [413.1, 662.9]	0.027
Systolic vorticity (1/s)	499.7 [377.1, 671.4]	396.5 [304.3, 586.6]	0.032
Diastolic vorticity (1/s)	481.2 [417.4, 624.1]	433.3 [331.9, 530.6]	0.636
Peak E-wave vorticity (1/s)	482.7 [421.7, 623.8]	455.9 [344.3, 522.0]	0.243
Peak A-wave vorticity (1/s)	478.7 [402.7, 629.3]	394.9 [318.6, 570.7]	0.282

The data are presented as the median [IQR]. IQR = [25th percentile, 75th percentile]. 4D, four dimensional; D-TGA, dextro-transposition of the great arteries; KEi_{EDV}, kinetic energy normalized to EDV; Peak systolic KEi_{EDV}, peak KEi_{EDV} of blood flow during systole; Systolic KEi_{EDV}, average KEi_{EDV} of blood flow during systole; Peak E-wave KEi_{EDV}, peak KEi_{EDV} of blood flow during early filling; Peak A-wave KEi_{EDV}, peak KEi_{EDV} of blood flow during late filling; EDV, end-diastolic volume; IQR, interquartile range.

Table 5 Univariate and multivariable linear regression analyses of the determinants of pulmonary artery obstruction

Parameters	Univariate analysis		Stepwise multivariable analysis	
	r (95% CI)	P value	β (95% CI)	P value
RV direct flow (%)	–0.14 (–7.84, 7.57)	0.971	–	–
RV retained inflow (%)	–6.17 (–13.56, 1.21)	0.098	–	–
RV delayed ejection flow (%)	3.12 (–4.50, 10.75)	0.411	–	–
RV residual volume (%)	4.07 (–3.50, 11.64)	0.281	–	–
Average KEi_{EDV} (μJ/mL)	12.64 (6.41, 18.86)	<0.001	–	–
Peak systolic KEi_{EDV} (μJ/mL)	8.45 (1.37, 15.53)	0.021	–	–
Systolic KEi_{EDV} (μJ/mL)	10.54 (3.83, 17.25)	0.003	–	–
Diastolic KEi_{EDV} (μJ/mL)	10.81 (4.16, 17.47)	0.002	13.54 (7.59, 19.49)	<0.001
Peak E-wave KEi_{EDV} (μJ/mL)	10.29 (3.53, 17.05)	0.004	105.26 (47.32, 163.21)	<0.001
Peak A-wave KEi_{EDV} (μJ/mL)	9.32 (2.38, 16.26)	0.010	–49.36 (–92.58, –6.14)	0.027
Average vorticity (1/s)	3.03 (–4.61, 10.66)	0.425	–56.37 (–84.17, –28.57)	<0.001
Peak systolic vorticity (1/s)	4.57 (–2.97, 12.10)	0.226		
Systolic vorticity (1/s)	2.28 (–5.39, 9.94)	0.549	–	–
Diastolic vorticity (1/s)	1.80 (–5.88, 9.49)	0.636	–	–
Peak E-wave vorticity (1/s)	1.71 (–5.97, 9.39)	0.653	–	–
Peak A-wave vorticity (1/s)	2.41 (–5.25, 10.07)	0.527	–	–

CI, confidence interval; RV, right ventricle; KEi_{EDV}, kinetic energy normalized to EDV; Peak systolic KEi_{EDV}, peak KEi_{EDV} of blood flow during systole; Systolic KEi_{EDV}, average KEi_{EDV} of blood flow during systole; Peak E-wave KEi_{EDV}, peak KEi_{EDV} of blood flow during early filling; Peak A-wave KEi_{EDV}, peak KEi_{EDV} of blood flow during late filling; EDV, end-diastolic volume.

Table 6 Intra and inter-observer variability for the blood flow components, kinetic energy and vorticity parameters

Parameters	Intra-observer (n=10)		Inter-observer (n=10)	
	ICC (%)	COV	ICC (%)	COV
LV				
Direct flow (%)	92.5	4.9	94.3	4.4
Retained inflow (%)	95.4	3.4	87.1	9.3
Delayed ejection flow (%)	89.1	7.9	93.4	6.5
Residual volume (%)	87.7	11.5	84.9	13.4
Average KEi_{EDV} (μJ/mL)	97.4	2.7	95.4	6.4
Peak systolic KEi_{EDV} (μJ/mL)	92.3	5.8	90.1	9.8
Systolic KEi_{EDV} (μJ/mL)	93.7	7.8	86.7	13.5
Diastolic KEi_{EDV} (μJ/mL)	92.8	4.7	87.7	10.3
Peak E-wave KEi_{EDV} (μJ/mL)	92.5	8.1	85.4	11.5
Peak A-wave KEi_{EDV} (μJ/mL)	96.8	3.5	90.5	4.6
Average vorticity (1/s)	94.3	4.5	92.5	9.3
Systolic vorticity (1/s)	92.6	6.7	89.3	13.5
Diastolic vorticity (1/s)	89.7	8.7	94.1	5.2
Peak E-wave vorticity (1/s)	94.1	4.9	92.4	6.3
Peak A-wave vorticity (1/s)	96.8	4.6	96.8	4.7
RV				
Direct flow (%)	90.5	10.3	89.6	12.6
Retained inflow (%)	92.7	8.7	90.3	10.5
Delayed ejection flow (%)	95.8	8.7	90.5	9.4
Residual volume (%)	96.3	5.1	94.7	4.9
Average KEi_{EDV} (μJ/mL)	99.8	3.4	91.3	7.5
Peak systolic KEi_{EDV} (μJ/mL)	95.6	6.4	85.6	13.1
Systolic KEi_{EDV} (μJ/mL)	92.3	8.5	91.4	6.8
Diastolic KEi_{EDV} (μJ/mL)	95.4	5.1	85.7	11.3
Peak E-wave KEi_{EDV} (μJ/mL)	95.4	4.9	86.2	11.3
Peak A-wave KEi_{EDV} (μJ/mL)	99.7	2.6	91.3	10.0
Average vorticity (1/s)	95.1	6.5	95.4	6.4
Systolic vorticity (1/s)	92.4	5.8	87.7	10.1
Diastolic vorticity (1/s)	96.3	7.3	95.3	6.7
Peak E-wave vorticity (1/s)	95.6	6.1	94.3	5.6
Peak A-wave vorticity (1/s)	98.4	4.3	92.1	7.9

ICC, intraclass correlation coefficient; COV, coefficient of variation; LV, left ventricle; KEi_{EDV}, kinetic energy normalized to EDV; Peak systolic KEi_{EDV}, peak KEi_{EDV} of blood flow during systole; Systolic KEi_{EDV}, average KEi_{EDV} of blood flow during systole; Peak E-wave KEi_{EDV}, peak KEi_{EDV} of blood flow during early filling; Peak A-wave KEi_{EDV}, peak KEi_{EDV} of blood flow during late filling; RV, right ventricle; EDV, end-diastolic volume.

In this study, we observed significantly reduced levels of LV systolic vorticity and peak A-wave vorticity in the patient group compared to the control group. These findings suggest that myocardial fibrosis and abnormal preload might have contributed to inefficient blood flow transmission in our study cohort (33). Further research needs to be conducted to explore the potential relationship between 4D flow hemodynamic parameters and fibrosis, which could help elucidate the underlying mechanisms of myocardial fibrosis.

This study did not find any significant differences in the RV vorticity parameters between the D-TGA patients and controls. The formation of the physiologic vortex has been hypothesized to create efficient flow pathways, minimizing turbulence and EL, and potentially reflecting the heart's adaptability to changing conditions. The formation of the RV diastolic vortex ring could not be accurately quantified using 4D flow CMR imaging. The mechanism of RV vortex ring transmission requires further research.

The relationship between RV hemodynamics and pulmonary artery abnormalities

Santens *et al.* (17) reported that pulmonary artery stenosis was frequently found in 234 of 289 patients, the stenosis was severe (15 patients, 6.4%). The obstruction was usually located at the bifurcation of the pulmonary artery (158 patients, 68%) in a 35-year follow-up study. Delaney *et al.* (34) reported that inefficient pulmonary artery flow might be an important predictor of RV afterload in D-TGA patients. Conversely, with an RV mass and a contractile reserve of approximately one-third of the LV, the RV output is highly sensitive to increases in afterload. Thus, the assessment of RV hemodynamics is particularly important in D-TGA patients. Our previous research also found that RV systolic and diastolic dysfunction highly prevalent in pediatric TOF patients during preserved RVEF (35). In our study, the RV systolic vorticity and peak E-wave KEi_{EDV} of the pulmonary stenosis group were significantly higher than those of the non-pulmonary stenosis group. The evidence from this study showed that this efficient hemodynamics are sensitive makers and might contribute to the adaptive remodeling of the RV.

Progressive obstruction in pulmonary circulation can lead to pressure loading in the RV, resulting in varying degrees of chronic pressure overload. As a result, multiple interventions may be necessary to reduce the pressure load on the RV, including balloon dilatation and stenting (16). In our study, all parameters related to the RV KE_{iEDV} were identified as independent predictors of pulmonary artery obstruction through the univariate analysis. Further, the RV diastolic KE_{iEDV} parameters and RV average vorticity were found to be risk factors for pulmonary artery obstruction in the multivariable model. Our research established a non-invasive RV hemodynamic model that can be used to optimize management strategies for the best long-term outcomes in D-TGA patients. We found acceptable inter- and intra-observer reproducibility in the biventricular hemodynamics measurements of the flow components, KE, and vorticity. This study has shown that the reproducibility of biventricular hemodynamics measurements is feasible, which is consistent with findings from previous large cohort studies on normal biventricular hemodynamics (29,32).

Limitations

This study had a number of limitations. This was a single-center prospective study; thus, further research needs to be conducted at multiple centers and with multiple vendors. The use of sedation for children aged under 8 years old (which occurred in 6 cases) was indicated by our institution protocol. However, the sedative effect might have altered the flow hemodynamics in these D-TGA patients. We cannot exclude the possibility of referral bias, although all the patients were asymptomatic. Several patients were removed from the study due to inadequate image quality, resulting from the long scan of the 4D flow sequence. Sotelo *et al.* (35) analyzed hemodynamic parameters in the aortas of healthy volunteers and patients with D-TGA, and found a relationship between the velocity angle and aortic root dilatation in the patients with D-TGA. In our study, 25 (73%) patients had neo-aortic root dilation. Unfortunately, we did not use 4D flow to evaluate the progress of the aortic root dilatation. We will compare the hemodynamics of aortic root dilatation and arterial-ventricular interaction in a further study (36). We normalized KE to EDV, as we did in our previous study (20). However, some studies have normalized KE to SV (31). The Bernoulli equation for pressure gradient quantification provides an estimate of the flow inside the ventricular outflow tract by echocardiography and can be used as a method for non-invasive evaluation in the next stage of research. In summary, we view this as a relatively preliminary study and note that multi-center, larger patient population studies need to be conducted.

Conclusions

We found that 4D flow biventricular hemodynamics were more sensitive markers than EF in postoperative D-TGA patients. The RV KEi_{EDV} parameters and RV average vorticity were risk factors for pulmonary artery obstruction.

Acknowledgments

Funding: This study was supported by grants from the National Key Clinical Specialties Construction Program, Innovative Research Team of High-Level Local Universities in Shanghai, National Natural Science Foundation of China (No. 82171902), the Shanghai Committee of Science and Technology (Nos.17411965400 and 22TS1400800), and the SJTU Trans-Med Awards Research (No. 20220101).

Footnote

Reporting Checklist: The authors have completed the STROBE reporting checklist. Available at https://qims.amegroups.com/article/view/10.21037/qims-24-840/rc

Conflicts of Interest: All authors have completed the ICMJE uniform disclosure form (available at https://qims.amegroups.com/article/view/10.21037/qims-24-840/coif). The authors have no conflicts of interest to declare.

Ethical Statement: The authors are accountable for all aspects of the work, including ensuring that any questions related to the accuracy or integrity of any part of the work have been appropriately investigated and resolved. The study was conducted in accordance with the Declaration of Helsinki (as revised in 2013). The study was approved by the Institutional Medical Ethics Committee of Shanghai Children's Medical Center (No. SCMCIRB-K2022.49-1). All the patients or their legal guardians and the healthy subjects provided written informed consent.

References

1. Fraser CD Jr. The Neonatal Arterial Switch Operation: Technical Pearls. Semin Thorac Cardiovasc Surg Pediatr Card Surg Annu 2017;20:38-42.
2. Lo Rito M, Fittipaldi M, Haththotuwa R, Jones TJ, Khan N, Clift P, Brawn WJ, Barron DJ. Long-term fate of the aortic valve after an arterial switch operation. J Thorac Cardiovasc Surg 2015;149:1089-94.
3. Prifti E, Crucean A, Bonacchi M, Bernabei M, Murzi B, Luisi SV, Vanini V. Early and long term outcome of the arterial switch operation for transposition of the great arteries: predictors and functional evaluation. Eur J Cardiothorac Surg 2002;22:864-73.
4. McMahon CJ, Ravekes WJ, Smith EO, Denfield SW, Pignatelli RH, Altman CA, Ayres NA. Risk factors for neo-aortic root enlargement and aortic regurgitation following arterial switch operation. Pediatr Cardiol 2004;25:329-35.
5. Helsen F, Claus P, Van De Bruaene A, Claessen G, La Gerche A, De Meester P, Claeys M, Gabriels C, Petit T, Santens B, Troost E, Voigt JU, Bogaert J, Budts W. Advanced Imaging to Phenotype Patients With a Systemic Right Ventricle. J Am Heart Assoc 2018;7:e009185.
6. Canan A, Ashwath R, Agarwal PP, François C, Rajiah P. Multimodality Imaging of Transposition of the Great Arteries. Radiographics 2021;41:338-60.
7. Fogel MA, Anwar S, Broberg C, Browne L, Chung T, Johnson T, Muthurangu V, Taylor M, Valsangiacomo-Buechel E, Wilhelm C. Society for Cardiovascular Magnetic Resonance/European Society of Cardiovascular Imaging/American Society of Echocardiography/Society for Pediatric Radiology/North American Society for Cardiovascular Imaging Guidelines for the Use of Cardiac Magnetic Resonance in Pediatric Congenital and Acquired Heart Disease: Endorsed by The American Heart Association. Circ Cardiovasc Imaging 2022;15:e014415.
8. Demirkiran A, van Ooij P, Westenberg JJM, Hofman MBM, van Assen HC, Schoonmade LJ, Asim U, Blanken CPS, Nederveen AJ, van Rossum AC, Götte MJW. Clinical intra-cardiac 4D flow CMR: acquisition, analysis, and clinical applications. Eur Heart J Cardiovasc Imaging 2022;23:154-65.
9. Tang M, Zhang F, Liu B, Liu Q, Qi W, Tang M, Luo Y, Chen J. Assessment of Pulmonary Arteries Hemodynamics and Its Relationship With Cardiac Remodeling and Myocardial Fibrosis in Athletes With Four-Dimensional Flow MRI. J Magn Reson Imaging 2024;60:377-87.
10. Garcia J, Barker AJ, Markl M. The Role of Imaging of

Flow Patterns by 4D Flow MRI in Aortic Stenosis. JACC Cardiovasc Imaging 2019;12:252-66.
11. Kamphuis VP, Elbaz MSM, van den Boogaard PJ, Kroft LJM, van der Geest RJ, de Roos A, Helbing WA, Blom NA, Westenberg JJM, Roest AAW. Disproportionate intraventricular viscous energy loss in Fontan patients: analysis by 4D flow MRI. Eur Heart J Cardiovasc Imaging 2019;20:323-33.
12. Sjöberg P, Bidhult S, Bock J, Heiberg E, Arheden H, Gustafsson R, Nozohoor S, Carlsson M. Disturbed left and right ventricular kinetic energy in patients with repaired tetralogy of Fallot: pathophysiological insights using 4D-flow MRI. Eur Radiol 2018;28:4066-76.
13. Kiener A, Kelleman M, McCracken C, Kochilas L, St Louis JD, Oster ME. Long-Term Survival After Arterial Versus Atrial Switch in d-Transposition of the Great Arteries. Ann Thorac Surg 2018;106:1827-33.
14. van der Palen RLF, Deurvorst QS, Kroft LJM, van den Boogaard PJ, Hazekamp MG, Blom NA, Lamb HJ, Westenberg JJM, Roest AAW. Altered Ascending Aorta Hemodynamics in Patients After Arterial Switch Operation for Transposition of the Great Arteries. J Magn Reson Imaging 2020;51:1105-16.
15. van der Palen RLF, van der Bom T, Dekker A, Tsonaka R, van Geloven N, Kuipers IM, Konings TC, Rammeloo LAJ, Ten Harkel ADJ, Jongbloed MRM, Koolbergen DR, Mulder BJM, Hazekamp MG, Blom NA. Progression of aortic root dilatation and aortic valve regurgitation after the arterial switch operation. Heart 2019;105:1732-40.
16. Terol Espinosa de Los Monteros C, Van der Palen RLF, Hazekamp MG, Rammeloo L, Jongbloed MRM, Blom NA, Harkel ADJT. Oxygen Uptake Efficiency Slope is Strongly Correlated to VO2peakLong-Term After Arterial Switch Operation. Pediatr Cardiol 2021;42:866-74.
17. Santens B, Van De Bruaene A, De Meester P, Gewillig M, Troost E, Claus P, Bogaert J, Budts W. Outcome of arterial switch operation for transposition of the great arteries. A 35-year follow-up study. Int J Cardiol 2020;316:94-100.
18. Bissell MM, Raimondi F, Ait Ali L, Allen BD, Barker AJ, Bolger A, et al. 4D Flow cardiovascular magnetic resonance consensus statement: 2023 update. J Cardiovasc Magn Reson 2023;25:40.
19. Stoll VM, Hess AT, Rodgers CT, Bissell MM, Dyverfeldt P, Ebbers T, Myerson SG, Carlhäll CJ, Neubauer S. Left Ventricular Flow Analysis. Circ Cardiovasc Imaging 2019;12:e008130.
20. Zhao X, Hu L, Leng S, Tan RS, Chai P, Bryant JA, Teo LLS, Fortier MV, Yeo TJ, Ouyang RZ, Allen JC, Hughes M, Garg P, Zhang S, van der Geest RJ, Yip JW, Tan TH, Tan JL, Zhong Y, Zhong L. Ventricular flow analysis and its association with exertional capacity in repaired tetralogy of Fallot: 4D flow cardiovascular magnetic resonance study. J Cardiovasc Magn Reson 2022;24:4.
21. Garcia J, Larose E, Pibarot P, Kadem L. On the evaluation of vorticity using cardiovascular magnetic resonance velocity measurements. J Biomech Eng 2013;135:124501.
22. Zhao X, Leng S, Tan RS, Chai P, Yeo TJ, Bryant JA, Teo LLS, Fortier MV, Ruan W, Low TT, Ong CC, Zhang S, van der Geest RJ, Allen JC, Hughes M, Garg P, Tan TH, Yip JW, Tan JL, Zhong L. Right ventricular energetic biomarkers from 4D Flow CMR are associated with exertional capacity in pulmonary arterial hypertension. J Cardiovasc Magn Reson 2022;24:61.
23. Stone ML, Schäfer M, DiMaria MV, von Alvensleben JC, Campbell DN, Jaggers J, Mitchell MB. Diastolic inflow is associated with inefficient ventricular flow dynamics in Fontan patients. J Thorac Cardiovasc Surg 2022;163:1195-207.
24. Kamphuis VP, Westenberg JJM, van der Palen RLF, van den Boogaard PJ, van der Geest RJ, de Roos A, Blom NA, Roest AAW, Elbaz MSM. Scan-rescan reproducibility of diastolic left ventricular kinetic energy, viscous energy loss and vorticity assessment using 4D flow MRI: analysis in healthy subjects. Int J Cardiovasc Imaging 2018;34:905-20.
25. Rutkowski DR, Barton G, François CJ, Bartlett HL, Anagnostopoulos PV, Roldán-Alzate A. Analysis of cavopulmonary and cardiac flow characteristics in fontan Patients: Comparison with healthy volunteers. J Magn Reson Imaging 2019;49:1786-99.
26. Kamphuis VP, Roest AAW, van den Boogaard PJ, Kroft LJM, Lamb HJ, Helbing WA, Blom NA, Westenberg JJM, Elbaz MSM. Hemodynamic interplay of vorticity, viscous energy loss, and kinetic energy from 4D Flow MRI and link to cardiac function in healthy subjects and Fontan patients. Am J Physiol Heart Circ Physiol 2021;320:H1687-98.
27. Schuwerk R, Freitag-Wolf S, Krupickova S, Gabbert DD, Uebing A, Langguth P, Voges I. Ventricular and atrial function and deformation is largely preserved after arterial switch operation. Heart 2021;107:1644-50.
28. Grotenhuis HB, Cifra B, Mertens LL, Riessenkampff E, Manlhiot C, Seed M, Yoo SJ, Grosse-Wortmann L. Left ventricular remodelling in long-term survivors after the arterial switch operation for transposition of the great arteries. Eur Heart J Cardiovasc Imaging 2019;20:101-7.
29. Zhao X, Tan RS, Garg P, Chai P, Leng S, Bryant JA, et al.

Age- and sex-specific reference values of biventricular flow components and kinetic energy by 4D flow cardiovascular magnetic resonance in healthy subjects. J Cardiovasc Magn Reson 2023;25:50.
30. Bolger AF, Heiberg E, Karlsson M, Wigström L, Engvall J, Sigfridsson A, Ebbers T, Kvitting JP, Carlhäll CJ, Wranne B. Transit of blood flow through the human left ventricle mapped by cardiovascular magnetic resonance. J Cardiovasc Magn Reson 2007;9:741-7.
31. Callaghan FM, Burkhardt B, Valsangiacomo Buechel ER, Kellenberger CJ, Geiger J. Assessment of ventricular flow dynamics by 4D-flow MRI in patients following surgical repair of d-transposition of the great arteries. Eur Radiol 2021;31:7231-41.
32. Hu LW, Xiang Y, Qin SY, Ouyang RZ, Liu JL, Peng YF, Xie WH, Zhang Y, Liu H, Zhong YM. Vortex formation time as an index of left ventricular filling efficiency: comparison between children volunteers and patients with tetralogy of Fallot. Transl Pediatr 2022;11:869-81.
33. Burkhardt BEU, Kellenberger CJ, Franzoso FD, Geiger J, Oxenius A, Valsangiacomo Buechel ER. Right and Left Ventricular Strain Patterns After the Atrial Switch Operation for D-Transposition of the Great Arteries-A Magnetic Resonance Feature Tracking Study. Front Cardiovasc Med 2019;6:39.
34. Delaney M, Cleveland V, Mass P, Capuano F, Mandell JG, Loke YH, Olivieri L. Right ventricular afterload in repaired D-TGA is associated with inefficient flow patterns, rather than stenosis alone. Int J Cardiovasc Imaging 2022;38:653-62.
35. Sotelo J, Valverde I, Martins D, Bonnet D, Boddaert N, Pushparajan K, Uribe S, Raimondi F. Impact of aortic arch curvature in flow haemodynamics in patients with transposition of the great arteries after arterial switch operation. Eur Heart J Cardiovasc Imaging 2022;23:402-11.
36. Ebel S, Köhler B, Aggarwal A, Preim B, Behrendt B, Jung B, Gohmann RF, Riekena B, Borger M, Lurz P, Denecke T, Grothoff M, Gutberlet M. Comparison of aortic blood flow rotational direction in healthy volunteers and patients with bicuspid aortic valves using volumetric velocity-sensitive cardiovascular magnetic resonance imaging. Quant Imaging Med Surg 2023;13:7973-86.

Cite this article as: Hu LW, Liu XR, Ouyang RZ, Chen LJ, Sun AM, Guo C, Yao XF, Ma YY, Feng L, Wu TF, Wang Q, Zhong YM. Characteristics of altered biventricular hemodynamics after arterial switch operation for patients with d-transposition of the great arteries with preserved ejection fraction: a four-dimensional (4D) flow cardiovascular magnetic resonance (CMR) study. Quant Imaging Med Surg 2024;14(10):7200-7217. doi: 10.21037/qims-24-840